Research Article

Xuwu Luo, Guancheng Jiang*, Guoshuai Wang, Lili Yang, Yinbo He, Kaixiao Cui, and Jun Yang

Novel approach to improve shale stability using super-amphiphobic nanoscale materials in water-based drilling fluids and its field application

https://doi.org/10.1515/rams-2022-0003
received September 03, 2021; accepted October 18, 2021

Abstract: In this study, super-amphiphobic nano-silica nanoparticles (SA-NPs) were used to enhance the shale stabilization performance of water-based drilling fluids (WBDFs) by altering the surface wettability, preventing the capillary self-priming effect, and plugging the nano-micro pores of shale. The results of transmission electron microscopy, particle size distribution, and scanning electron microscopy characterization revealed that SA-NPs exhibited a nanoscale "coalesce" structure, which is composed of spherical particles joined together, and could form a nano-papillary structure on the shale surface. Due to the presence of nano-micro scale rough structures and ultra-low surface energy components, the shale treated by SA-NPS exhibited super-amphiphobic surface property in the contact angle test. Contact angles of water and hexadecane on the shale surface reached up to 154.13° and 151.34° after being treated with SA-NPs, respectively. Furthermore, the addition of 1% SA-NPs in WBDFs could reduce the linear swelling rate from 40.5 to 6.0%, increase the shale cuttings recovery percentages from 82.5 to 95.6%, increase the plugging rate of low permeability shale core from 81.25 to 94.00%, and raise the high-temperature and high-pressure uniaxial compressive strength from 3.45 to 4.87 MPa. Compared with the polyether amine and fumed nano-silica, the addition of SA-NPs produced the best performance. Based on the excellent shale stabilization performance of SA-NPs, a high-performance WBDF was developed and applied in Dagang Oilfield. During the drilling operation , no wellbore instability, sticking, and other complex situations occurred. The results indicate that SA-NPs could better address the issue of wellbore instability in shale formations and have a great application prospect in shale well drilling.

Keywords: super-amphiphobic surface, capillary force, shale formation, water-based drilling fluids, inhibition performance

1 Introduction

The rapid growth of global oil and gas demand and the depletion of conventional oil and gas resources have driven the rapid exploration and exploitation of unconventional oil and gas resources, especially shale oil and gas resources [1]. Characterized by rich clay mineral contents, developed bedding structures, and abundant nano-micro cracks and nanopores, shale has a strong amphiphilicity and capillary self-imbibition effect [2–4]. It spontaneously absorbs free water from drilling fluid under capillary forces. The resulting hydration swelling and dispersion of clay minerals thus widen cracks and reduce shale strength [5–7]. Therefore, in the drilling process of shale formation using water based-drilling fluids (WBDFs), wellbore instability, such as borehole shrinkage, spalling, and even collapse often occurs, greatly increases the drilling cost and even

* **Corresponding author: Guancheng Jiang,** State Key Laboratory of Petroleum Resources and Prospecting, China University of Petroleum (Beijing), Beijing 102249, People's Republic of China; Ministry of Education (MOE) Key Laboratory of Petroleum Engineering, China University of Petroleum (Beijing), Beijing 102249, People's Republic of China,
e-mail: m15600263100_1@163.com
Xuwu Luo: State Key Laboratory of Petroleum Resources and Prospecting, China University of Petroleum (Beijing), Beijing 102249, People's Republic of China; Western Drilling Engineering Company of PetroChina, Karamay 834099,
People's Republic of China
Guoshuai Wang, Lili Yang, Yinbo He, Kaixiao Cui, Jun Yang: State Key Laboratory of Petroleum Resources and Prospecting, China University of Petroleum (Beijing), Beijing 102249, People's Republic of China; Ministry of Education (MOE) Key Laboratory of Petroleum Engineering, China University of Petroleum (Beijing), Beijing 102249, People's Republic of China

severely restricts the exploration and development process of shale oil and gas resources [8,9].

To address the wellbore instability issue in shale formations, even though WBDFs with better inhibition property were developed, such as potassium chloride/partially hydrolyzed polyacrylamide (KCl/PHPA) drilling fluids, saturated brine drilling fluids, silicate-based drilling fluids, polyamine drilling fluids, and KCl/diamino hexane drilling fluids [10–15], they cannot maintain the wellbore stability well in shale formations. Therefore, invert emulsion drilling fluids (IEDFs), a type of water-in-oil emulsion drilling fluids, were used to drill shale formations [16]. Though excellent in wellbore stability and drilling efficiency in shale formations owing to the absence of contact between the wellbore rock and water phase [17], IEDFs show nonetheless inherent disadvantages, including difficulty in mud cakes clearing and cuttings handling, high post-treatment costs, and severe environmental pollution. To date, the use of IEDFs in many oilfields has been restricted by strict environmental protection laws and high costs [18–20]. Therefore, developing high-performance WBDFs to replace IEDFs against the above issues has become a research focus in the petroleum industry.

Studies have gradually pointed out that reducing capillary force and increasing rock hydrophobicity are beneficial to the wellbore stability of shale formations [21–23]. Shi et al. reported that compound surfactants (nonionic surfactant and fluorocarbon surfactant) in WBDFs could enhance the hydrophobicity of wellbore rocks and reduce the contact between free water in WBDFs and wellbore rock, thus improving wellbore stability [24]. Xu et al. synthesized a hydrophobic-modified polymer-based silica nanocomposite. It can make the shale surface more hydrophobic, thereby showing excellent shale inhibition performance [25]. Yue et al. optimized a surfactant combination (cetyl trimethyl ammonium bromide and sodium dodecylbenzene sulfonate) that can improve wellbore stability in shale formation by effectively reducing the surface tension of WBDFs or freshwater and increasing the contact angle with shale [26]. Nevertheless, being unable to form complete hydrophobic surfaces, much less super-hydrophobic ones, these surfactants or hydrophobic polymers can only increase the hydrophobic degree of rocks, and thus cannot effectively prevent water intrusion. Recently, nanomaterials such as fumed silica (SiO_2) nanoparticles (NPs), titanium dioxide (TiO_2) NPs, graphene oxide, and multi-walled carbon nanotubes (MCNTs) have also shown great potential in improving the wellbore stability of shale formations [27–30]. Because they can plug the nano-micro pores on the shale surface, they can avoid free water intrusion. However, these conventional nanomaterials are hydrophilic. They cannot change the wettability of the rock surface and prevent the capillary self-priming effect. Therefore, these conventional nanomaterials cannot effectively inhibit the surface hydration of the shale and prevent the intrusion of free water to the greatest extent. In comparison, super-amphiphobic nanomaterials have recently attracted significant attention due to their unique characteristics, which can simultaneously endow the solid surface with the characteristics of repelling water, oil, and organic liquid [31]. Moreover, it performs the functions of self-cleaning, self-healing, anti-corrosion, anti-pollution, and super-protection, consequently showing a wide application prospect in daily life, environmental protection, industrial production, medical treatment, military, and other aspects [32–36]. Fluorinated NPs are commonly used to construct super-amphiphilic surfaces [37–39]. Lu et al. directly mixed two kinds of TiO_2 of different particle sizes (60–200 and 21 nm) with 1*H*,1*H*,2*H*,2*H*-perfluorooctyltriethoxysilane to obtain an ethanol suspension of 1*H*,1*H*,2*H*,2*H*-perfluorooctyltriethoxysilane-coated TiO_2 nanoparticles, such that when applied to different substrate surfaces such as glass, steel, cotton fabrics, and paper, it shows super-amphiphobic [40]. Our group has previously synthesized a nanofluid from nano-silica, MCNTs, and trichloro (1*H*,1*H*,2*H*,2*H*-perfluorooctyl) silane, which can change the wettability of sandstone core surface from amphiphilic to amphiphobic [41].

In this study, a novel super-amphiphobic nanoscale material (SA-NPs), nano-silica grafted with amine groups and halothane segments, was employed to improve the wellbore stabilization performance of WBDFs in shale well drilling operations. The presence of amine groups contributes to the absorption on the shale surface. The nanoscale structure and halothane segments can improve nano-micro scale shale surface roughness, construct super-amphiphobic surface, and plug nano-micro pores. A flowchart of the procedure of this research is shown in Figure 1. First, the microstructure of SA-NPs was characterized through transmission electron microscopy (TEM) and particle size distribution measurement, and its influence on the shale surface microstructure was studied by scanning electron microscopy (SEM). Then, the wetting and interface characteristics of SA-NPs on the shale surface and glass capillary were investigated by the contact angle test and capillary force measurement. The shale stabilization performance of SA-NPs in WBDFs was further evaluated through the linear swelling test, hot-rolling recovery test, plugging rate test, and HTHP uniaxial compressive strength test. Meanwhile, the performance of SA-NPs was compared with that of polyether amine (PA) and fumed nano-silica to fully demonstrate the advantage of SA-NPs. Finally, with SA-NPs as the core treatment agent, a high-performance WBDF was prepared, evaluated, and applied on the oilfield.

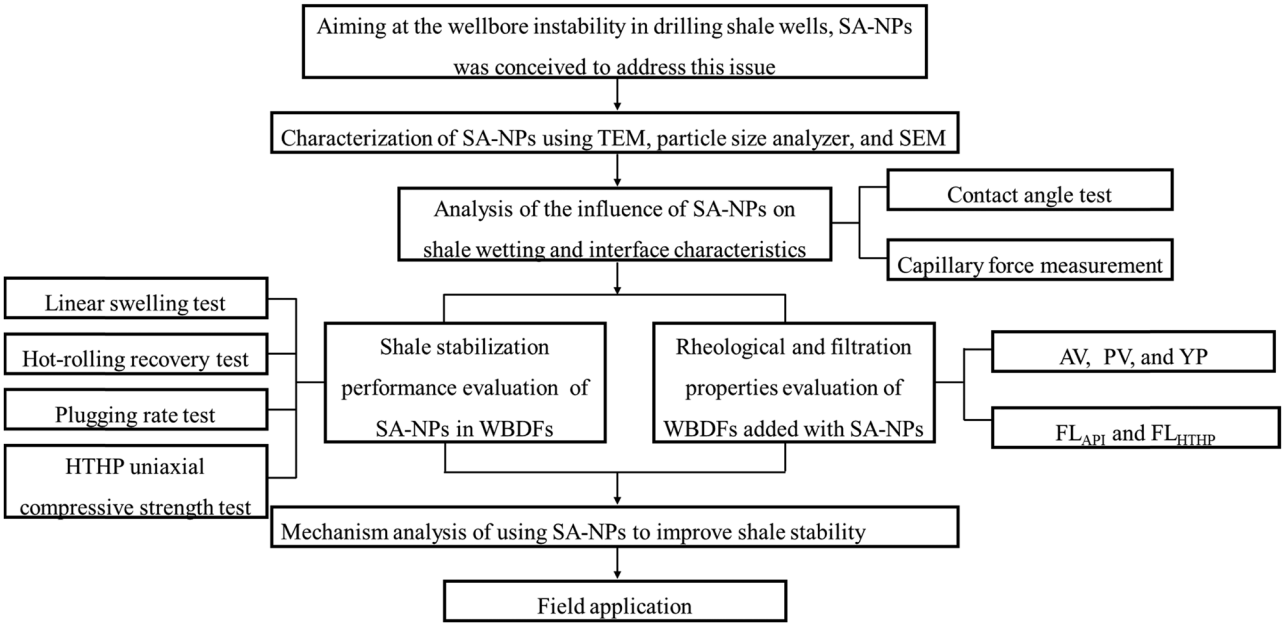

Figure 1: Flowchart of the procedure of this research.

2 Materials and methods

2.1 Materials

The super-amphiphobic nano-silica nanoparticles (SA-NPs), a commercial product provided by Shida Bocheng Technology Co., Ltd (Beijing, China), were synthesized by fluorination modification of fumed SiO_2 NPs. The chemical structure of the SA-NPs is shown in Figure 2. Poly dimethyldiallyl ammonium chloride (PDMDAAC), PA D-2000, SiO_2 with a diameter of 20 nm, KCl, sodium chloride (NaCl), and calcium chloride ($CaCl_2$) were purchased from Energy Chemical (Shanghai, China). In addition, Ethyl alcohol and hexadecane were purchased from Aladdin Chemical Inc. (Shanghai, China). The glass capillary tube with a radius of 0.15 mm was provided by Changzhou Kejing Glass Co., Ltd (Changzhou, China). Bentonite (consisting of 69.3% montmorillonite), shale cuttings, and a WBDF (ρ = 1.4 g·cm^{-3}) were supplied by China National Petroleum Corporation (CNPC) Western Drilling Engineering Co., Ltd (Karamay, China). The mineral compositions of the shale cuttings and formulation of WBDFs are shown in Tables 1 and 2, respectively.

2.2 Characterization of SA-NPs

The TEM images of SA-NPs were obtained by a JEM-2100 transmission electron microscope (Tokyo, Japan). The particle size distribution of SA-NPs was measured by a Malvern Zetasizer Nano ZS instrument (Malvern, England). In these tests, the concentration of the sample in ethyl alcohol was 0.1% w/v.

The influence of SA-NPs on the surface micro-morphology of shale was examined by a SU8010 scanning electron microscope (SEM; Tokyo, Japan). Specifically, in preparation of a dispersion, 0.3 g SA-NP powder was

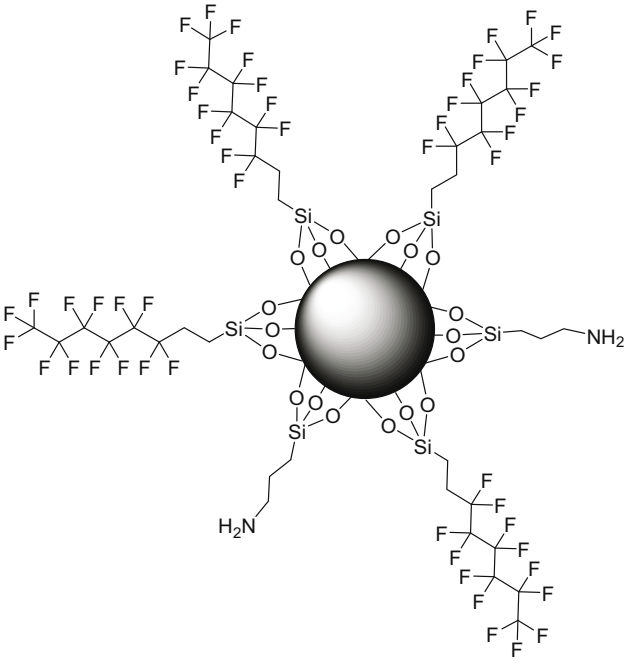

Figure 2: The chemical structure of the SA-SiO_2.

Table 1: Mineral composition of the shale cuttings

Component	Quartz	Potassium feldspar	Plagioclase	Calcite	Dolomite	Augite	Clay mineral
Content (%)	31.7	1.4	2.1	17.4	2.8	2.0	42.6

Table 2: Formulation of WBDFs

Additives	Composition (g)
Fresh water	300
Bentonite	3
NaOH	0.9
Filtrate reducer XZ-KGJ	6
Plugging agent XZ-FDJ	9
Plugging agent OSD-1	6
Lubricant JHRH-1	6
Potassium polyacrylamide KPAM	0.6
KCl	24
NaCl	60

dispersed in 10 mL of ethyl alcohol under ultrasonic treatment. The shale sample was subsequently immersed in the dispersion for 24 h and dried afterward in a vacuum oven at 70°C for 2 h for SEM testing.

2.3 Wetting and interface characteristics

2.3.1 Contact angle test

Generally, the solid surface is considered to be super-amphiphobic when it has contact angles with oil and water phases, both greater than 150° [42,43]. The contact angle was measured using the following procedure. The shale samples were first immersed in SA-NPs dispersion, SiO_2 dispersion, and commonly used shale inhibitors aqueous solutions separately for 24 h, and then dried in a blast drying oven at 80°C for 4 h. Then, hexadecane with a surface energy of 73.2 $mN{\cdot}m^{-1}$ and deionized (DI) water with a surface energy of 27.2 $mN{\cdot}m^{-1}$ were used as test liquids, respectively. The contact angle of the shale surface was at last determined by a JC2000D3 contact angle measuring instrument (Shanghai, China), in which the droplets volume of test liquid was set to 5 μL.

2.3.2 Capillary force measurement

The existence of lots of micro-nano pores in the shale surface brings natural capillary force that allows shale to spontaneously absorb water, which thereby affects wellbore stability. In this work, the nano-micro pores of shale are simulated by glass capillary tubes whose capillary forces were treated with different liquids and tested by the method shown in Figure 3. In this method, the glass capillary tubes were immersed in different test liquids for 1 h and dried in an oven at 80°C for 4 h. Then, the well-prepared glass capillaries were inserted vertically into DI water of the same height. The capillary force can be calculated using equation (1) [43].

$$p_c = \frac{2\sigma\cos\theta}{r}, \tag{1}$$

where p_c is the capillary force (Pa) measured at 25°C; σ is the surface tension (73.2 $mN{\cdot}m^{-1}$) of DI water; θ is the contact angle (°) of capillary inner surface; and r is the capillary radius (0.15 mm).

2.4 Shale stabilization performance evaluation

2.4.1 Linear swelling test

The linear swelling test was carried out to investigate the ability of WBDFs to inhibit the hydration swelling of shale. First, shale cuttings powder (5 g) was pressed

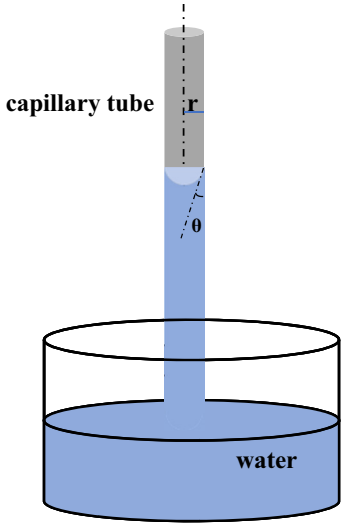

Figure 3: The schematic diagram of capillary force measurements.

into a cylindrical pellet under a pressure of 10 MPa for 5 min. Then, the pellet was installed in the CPZ-2 dual-channel linear swell meter (Qingdao, China), with 20 mL of drilling fluid filtrate added to immerse the shale cuttings pellet. Finally, the swelling height was recorded every 30 s for 24 h. Accordingly, the linear swelling rate is calculated using equation (2) [23].

$$\text{Linear swelling rate} = \frac{h_t - h_0}{h_0} \times 100\%, \tag{2}$$

where h_t is the final height (mm) of shale cuttings pellet after immersed in test liquid for a certain time t; and h_0 is the initial height (mm) of shale cuttings pellet.

2.4.2 Hot-rolling recovery test

The hot-rolling recovery test was conducted to investigate the ability of WBDFs to inhibit the hydration disintegration of shale cuttings at borehole temperature. First, 20 g shale cuttings (6–10 mesh) and 300 mL of drilling fluids were added to a sealed stainless steel aging jar and rolled at 140°C in a GW300-X roller oven (Qingdao, China) for 16 h. After cooling, the remaining shale cuttings were screened by a 40-mesh sieve, washed with clean water, and dried in a hot oven at 75°C for 24 h. The recovery percentage of shale cuttings is calculated according to equation (3).

$$\text{Recovery percentage} = \frac{m_1}{m_0} \times 100\%, \tag{3}$$

where m_1 is the remaining mass and m_0 is the original mass of the shale cuttings.

2.4.3 Plugging rate test

The plugging rate test was conducted to investigate the ability of WBDFs to plug the nano-micro pores and fractures of the shale. First, the positive permeability (K_i) of the original shale cores with kerosene being the fluid in the first place was examined using a JHMD-2 core dynamic damage evaluation instrument (Jingzhou, China). Then, the core was positively contaminated with different drilling fluids for 120 min under a pressure difference of 6 MPa and a confining pressure of 2 MPa. At last, the positive direction permeability (K_p) of the core was examined by using brine (4% NaCl) as the fluid, and the plugging rate (P_r) value is calculated using equation (4).

$$P_r = \frac{K_i - K_p}{K_i} \times 100\%. \tag{4}$$

2.4.4 HTHP uniaxial compressive strength test

The nature of wellbore instability is mechanical instability. Therefore, the influence of different mud samples on the artificial shale cores' strength was evaluated by the uniaxial compressive strength experiment. During the experiment, bentonite (20 g) was pressed into a columnar core under 15 MPa pressure for 15 min. Then, the bentonite core was placed in a stainless steel sealed kettle containing mud samples and immersed at a fixed pressure difference of 3.5 MPa and 90°C for 7 days (Figure 4). Uniaxial compressive strength measurement was conducted using a JHYL-1 dynamic core strength evaluation instrument (Jingzhou, China).

2.5 Rheological and fluid loss properties evaluation

The rheological properties of WBDFs were investigated by a ZNN-D6 six-speed rotational viscometer (Qingdao, China) whose readings at 300 and 600 rpm were recorded and marked as θ_{300} and θ_{600}, respectively. The rheological parameters were calculated by the following equations:

$$\text{AV} = 0.5\theta_{600}, \tag{5}$$

$$\text{PV} = \theta_{600} - \theta_{300}, \tag{6}$$

$$\text{YP} = 0.5(\theta_{300} - \text{PV}), \tag{7}$$

where AV is the apparent viscosity (mPa·s), PV is the plastic viscosity (mPa·s), and YP is the yield point (Pa).

The medium pressure filtration volume (FL_{API}) and HTHP filtration volume (FL_{HTHP}) were measured according to the method recommended by American Petroleum

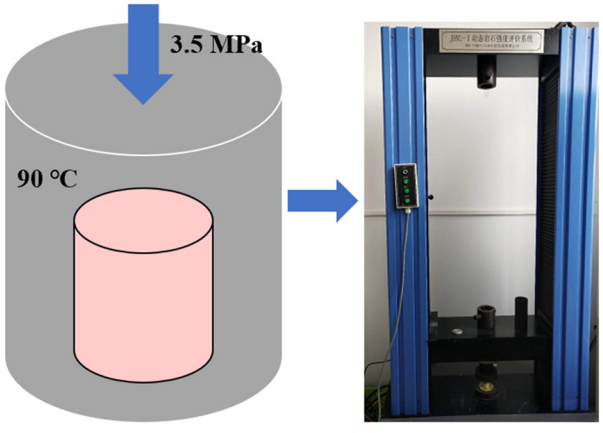

Figure 4: The schematic diagram of HTHP uniaxial compressive strength tests.

Institute (API). FL_{API} was measured by an SD-6 medium-pressure filtration apparatus (Qingdao, China) at a fixed pressure difference of 0.69 MPa and room temperature, in which the FL_{API} was recorded after 30 min since the beginning. FL_{HTHP} was measured by a GGS42-2A HTHP filtration apparatus (Qingdao, China) at a fixed pressure difference of 3.5 MPa and a temperature of 140°C.

3 Results and discussion

3.1 Characterization of SA-NPs

The construction of a nano-micro scale rough structure is one of the key elements to form a super-amphiphobic surface [44,45]. As shown in Figure 5, the microstructure and size of SA-NPs were demonstrated by the TEM and particle size distribution curve. In the TEM images of Figure 5a and b, SA-NPs exhibit a nanoscale "coalesce" structure composed of joint spherical particles, which is attributed to the association of hydrogen bonds between the amine groups grafted on the surface of SA-NPs. In Figure 5c, the particle size of SA-NPs distributes in the range from 70 to 200 nm with an average particle size of about 105.3 nm, meaning that SA-NPs are able to enter and plug shale nano-micro pores and cracks. On the other hand, the surface of the original shale presents a relatively smooth nano-micro scale structure, as shown in Figure 5d. After treatment with SA-NPs dispersion, lots of spherical particles are adsorbed and distributed on the surface of the treated shale in the form of uneven

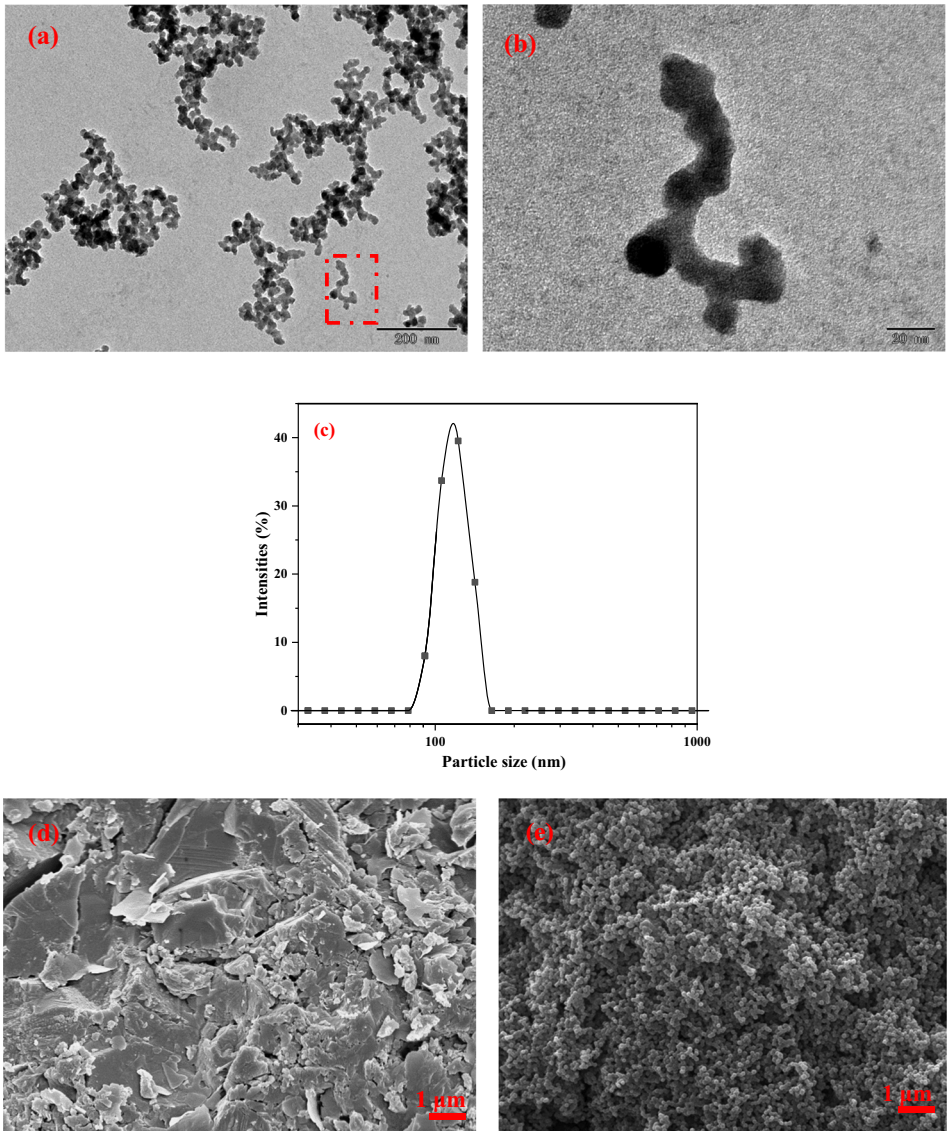

Figure 5: The microstructure and size of SA-NPs. TEM images of SA-NPs (a) and (b); particle size distribution of SA-NPs (c); SEM image of original shale surface (d); and SEM image of shale treated with SA-NPs (e).

aggregates, forming a nano-papillary structure (Figure 5e). This new structure, to a great extent, improves the roughness of the shale surface at the nano-micro scale. Simultaneously, SA-NPs used in our study have been pre-grafted with halothane segment and can present super-low surface energy components. Therefore, the shale treated by SA-NPs would achieve super-amphiphobic surface property.

3.2 Contact angle test

Figure 6 shows water and oil phase contact angles on the shale surface before and after being treated with SA-NPs. In this test, DI water and hexadecane were used as water and oil contact phases, respectively. Before the treatment, the contact angles of DI water and hexadecane on the original shale surface were only 14.65° and 5.09°, respectively, as shown in Figure 6a and b, indicating an amphiphilic property. Whereas, as shown in Figure 6c and d, after tiny amounts of SA-NPs treatment, the two contact angles drastically raised to 154.13° and 151.34°, respectively. This change in the surface wettability marked the forming of super-amphiphobic property. This experiment illustrates that the amphiphilic surface would become a super-amphiphobic surface if the shale is immersed in SA-NPs suspension for a period, which is suitable for the actual drilling situation. The super-amphiphobic property enables the shale surface to perform self-cleaning and anti-polluting activities, which effectively prevents contact with water and organic liquid molecules, and thereby, inhibits hydration swelling and mineral particle cohesion.

In addition, the contact angles between the water phase and shale surface after treated with several commonly used shale inhibitors were also measured (Figure 7). Wherein, KCl (10.32°) and PDMDAAC (11.41°) can be observed to slightly reduce the contact angle with the water phase, which can be related to the increase in hydrophilicity of the shale brought by the cation groups absorbed on the shale surface. On the contrary, PA (27.34°) and SiO_2 (31.72°) slightly increase contact angle, even then it is always less than 32°. It is evident that commonly used inhibitors cannot alter the wettability of shale, and it remains similar to the hydrophilic property. In contrast, SA-NPs (154.13°) generate a super-hydrophobic surface on shale playing a rather different role. The inability of these common inhibitors to avoid capillary self-priming effect and shale's surface hydration results from the failure of avoiding the association of water molecules with the shale surface and pores will be further verified in the following capillary force measurement experiment.

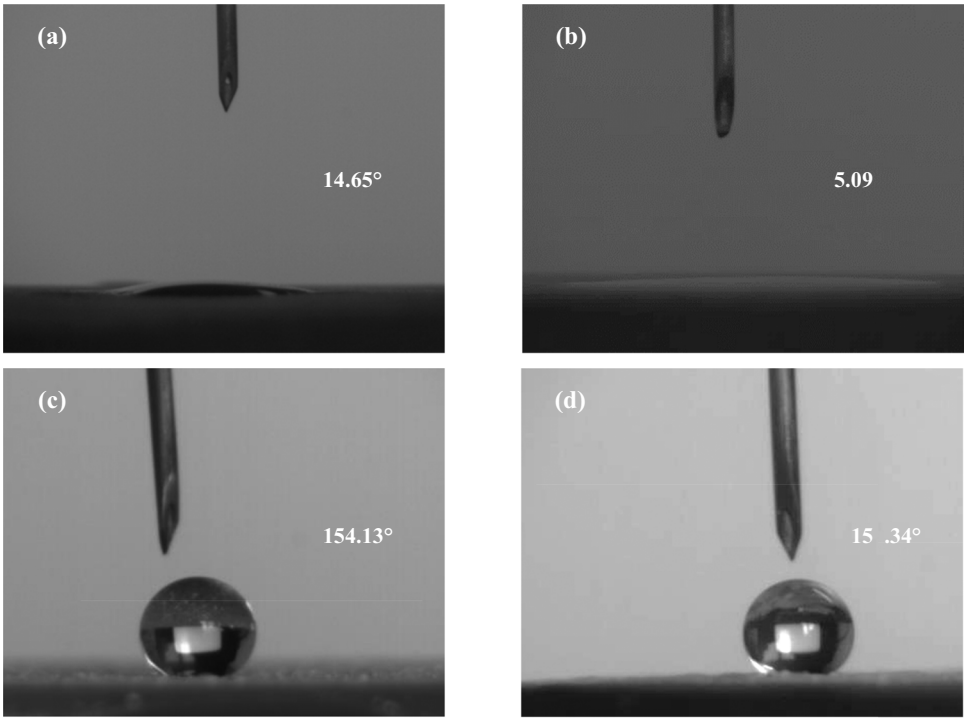

Figure 6: DI water and hexadecane contact angles on shale surface before and after being treated with SA-NPs. Water droplet on original shale surface (a); hexadecane droplet on original shale surface (b); water droplet on shale surface treated with SA-NPs (c); and hexadecane droplet on shale surface treated with SA-NPs (d).

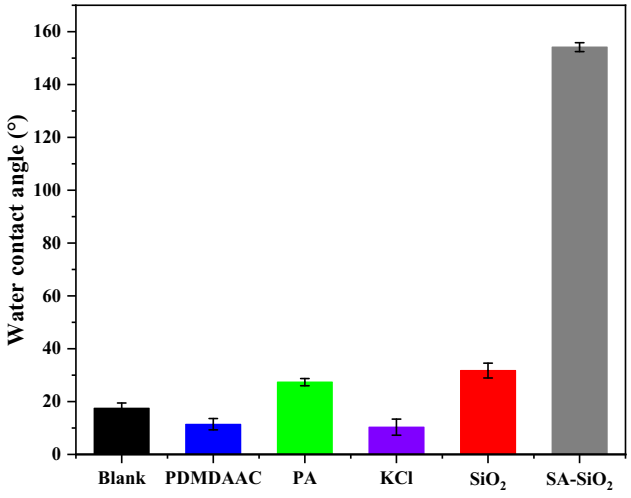

Figure 7: The water phase contact angle of the shale treated with SA-NPs and commonly used inhibitors solution at a concentration of 3 wt%.

3.3 Capillary force measurements

Capillary force measurement was conducted to evaluate the ability of SA-NPs and commonly used inhibitors to avoid capillary self-priming. Typically, a greater capillary force means a stronger self-priming ability, while a negative capillary force indicates a conversion from the capillary attraction force into the capillary repulsion force. Figure 8 shows the capillary forces of the glass capillary tube treated with SA-NPs and commonly used inhibitors solutions, with results ordering as follows: SA-NPs (−833.78 kPa) < SiO_2 (789.62 kPa) < PA (799.13 kPa) < KCl (817.43 kPa) < PDMDAAC (817.44 kPa) < Blank (880.73 kPa). While the result indicates a conventional inhibitors' ability to slightly reduce the capillary force, the effect of mitigating water intruding is minimal yet beneficial. Nevertheless, the negative capillary force exhibited by SA-NPs illustrates its ability to alter and turn the capillary attraction force into the capillary repelling force that avoids capillary self-priming and water-blocking phenomenon. The contact angle test and capillary force test verified the ability of SA-NPs to reverse the wettability of the shale surface and avoid capillary self-priming. Theoretically, this ability will greatly improve the stability of the shale. Then, we further evaluated the ability of SA-NPs to stabilize shale in WBDFs.

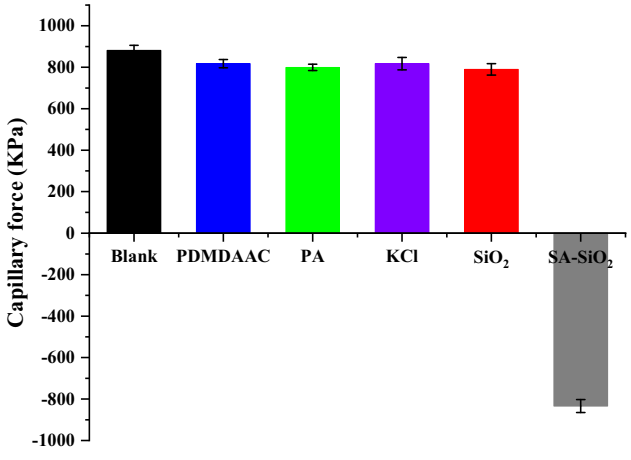

Figure 8: Capillary forces of the glass capillary tube treated with SA-NPs and commonly used inhibitors.

3.4 Shale stabilization performance of SA-NPs in WBDFs

3.4.1 Linear swelling test and hot-rolling recovery test

The inhibition performance of four samples, including fresh tap water, WBDFs, WBDFs added with 2% PA (PA-WBDFs), and WBDFs added with 1% SA-NPs (SA-WBDFs), were tested for comparison and the corresponding experimental results are shown in Figures 9 and 10. After immersed in water and WBDFs for 24 h, the shale cuttings pellet has linear swelling rates reaching as high as 96 and 40.5%, respectively. These rates marked a severe swelling of shale cuttings in these two solutions especially in water that harms borehole stability. As an effective shale inhibitor, PA can reduce the swelling degree to 13.5%. Nonetheless, this performance is still far from satisfactory, especially for good horizontal drillings. Therefore, the inhibiting performance of common shale inhibitors is not sufficient to impede

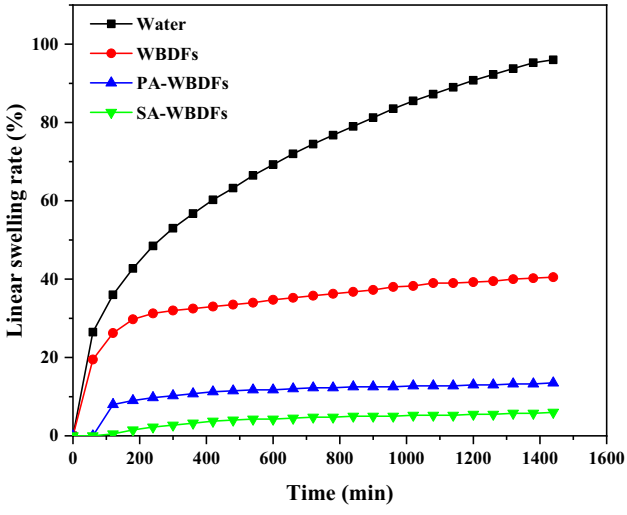

Figure 9: The linear swelling rate of shale cuttings powder in different WBDFs.

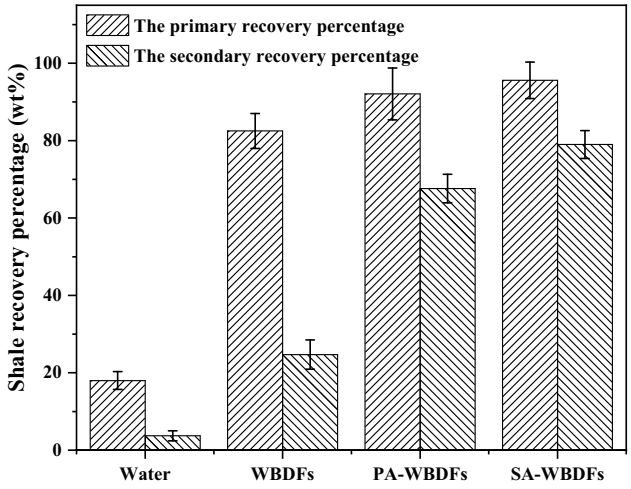

Figure 10: Recovery percentages of shale cuttings in different WBDFs.

borehole instability problems such as wellbore shrinkage. On the contrary, When SA-NPs were added instead, the linear swelling rate of SA-WBDFs was further reduced to 6%, indicating the superior inhibition performance of SA-NPs than that of PA inhibitor. After adding 1% SA-NPs to WBDFs, the primary recovery percentage and secondary recovery percentage increased from 82.5% and 24.7% to 95.6% and 79%, respectively, implying an effective absorption made by SA-SiO_2-NPs on shale surface to prevent shale hydration dispersion without degrading or falling due to high temperature and long duration. It is also worth noting that the shale recovery percentage of SA-WBDFs is the highest and better than that of PA-WBDFs, once again showing the excellent inhibition performance of SA-NPs.

3.4.2 Plugging rate test

The addition of nano-materials to WBDFs may potentially plug shale nano-micro pores and cracks and reduce the penetration of drilling fluid filtrate into the borehole rock, thereby reducing borehole instability [19]. The plugging rates of WBDFs, WBDFs with 1% SiO_2 (SiO_2-WBDFs), and SA-WBDFs for low permeability shale core are shown in Table 3. The addition of SiO_2 and SA-NPs could be easily observed to increase the plugging rates of WBDFs from 81.25 to 84.61% and then 94.00%, respectively. Compared to SiO_2, WBDFs with 1% SA-NPs demonstrated a better stabilizing ability as SA-NPs not only physically plug the shale pores, but also change the wettability of shale pore throats, thereby increasing the resistance of the liquid phase through pore throats.

Table 3: The plugging rate (P_r) of different WBDFs

Mud system	(K_i)/D	(K_p)/D	(P_r)/%
WBDFs	0.048	0.009	81.25
SiO_2-WBDFs	0.052	0.008	84.61
SA-WBDFs	0.050	0.003	94.00

3.4.3 HTHP uniaxial compressive strength test

The HTHP uniaxial compressive strength of bentonite cores immersed in different WBDFs is shown in Figure 11. Compared with the original bentonite core, the core strength decreases sharply from 8.89 to 1.82 MPa after immersion in clear water, indicating a great reduction in core strength in a water environment. Even though the reduction level in uniaxial compressive strength is relatively improved after replacing water with WBDFs, the result is far from satisfactory, especially when it comes to horizontal shale-well drilling. With the addition of PA, SiO_2, and SA-NPs, the uniaxial compressive strength of bentonite cores was stronger than that in the original drilling fluid, which increased to 4.12, 3.26, and 4.87 MPa, respectively. Therefore, it can be concluded that the addition of SA-NPs resulted in the highest uniaxial compressive strength. The reason behind this phenomenon is that while PA can only inhibit bentonite hydration swelling and SiO_2 can only physically plug core, SA-NPs not only simultaneously achieve these effects, but also reverse the

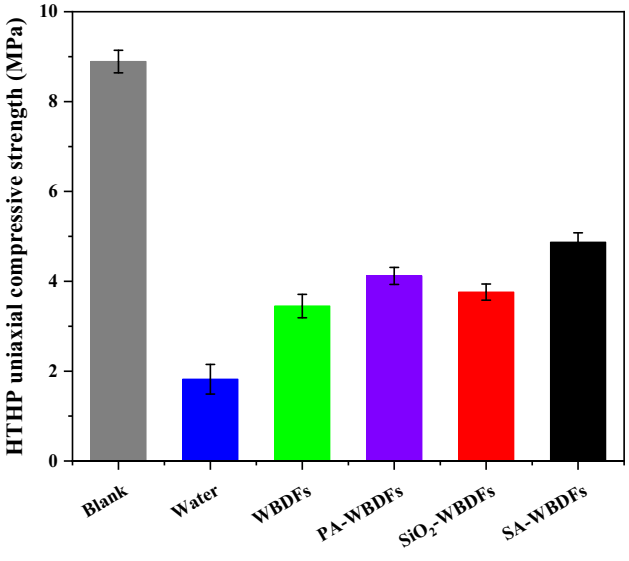

Figure 11: The HTHP uniaxial compressive strength of bentonite cores immersed in different WBDFs.

wettability of shale surface and pore throat. Thus, after absorption of SA-NPs, the core surface exhibits super-amphiphobic property, which prevents water molecules from forming hydrogen bonds with the bentonite surface, and effectively repels the intrusion of foreign liquid phases. Therefore, the SA-NPs are capable of inhibiting shale hydration swelling and disintegration, plugging nano-micro pores, and preventing foreign liquid intrusion, thus maintaining the shale strength and wellbore stability.

3.5 Rheological and filtration properties of SA-WBDFs

To explore the feasibility of using SA-WBDFs in actual drilling operations, the rheological and filtration properties under different pollution conditions were further evaluated. As shown in Figure 12a–c, AV, PV, and YP of SA-WBDFs and SA-WBDFs containing 10% NaCl, soil powder, and shale cutting powder are barely different before and after being aged at 140°C for 16 h, indicating the stable rheological properties of SA-WBDFs. The FL_{API} and FL_{HTHP} of SA-WBDFs before and after being contaminated by 10% NaCl, soil powder, and shale cutting powder are always less than 3 and 8 mL, respectively, illustrating the excellent filtration control ability and anti-pollution ability of the drilling fluid. Though there was a slight increase in AV, PV, and FL_{HTHP} when SA-WBDFs were contaminated with $CaCl_2$ due to the Ca^{2+} flocculation effect on the drilling fluid [46], the rheological parameters and filtration volume of SA-WBDFs were still within the API standard, satisfying drilling operation requirements. Therefore, SA-WBDFs can have excellent rheological fluid loss control performance during the

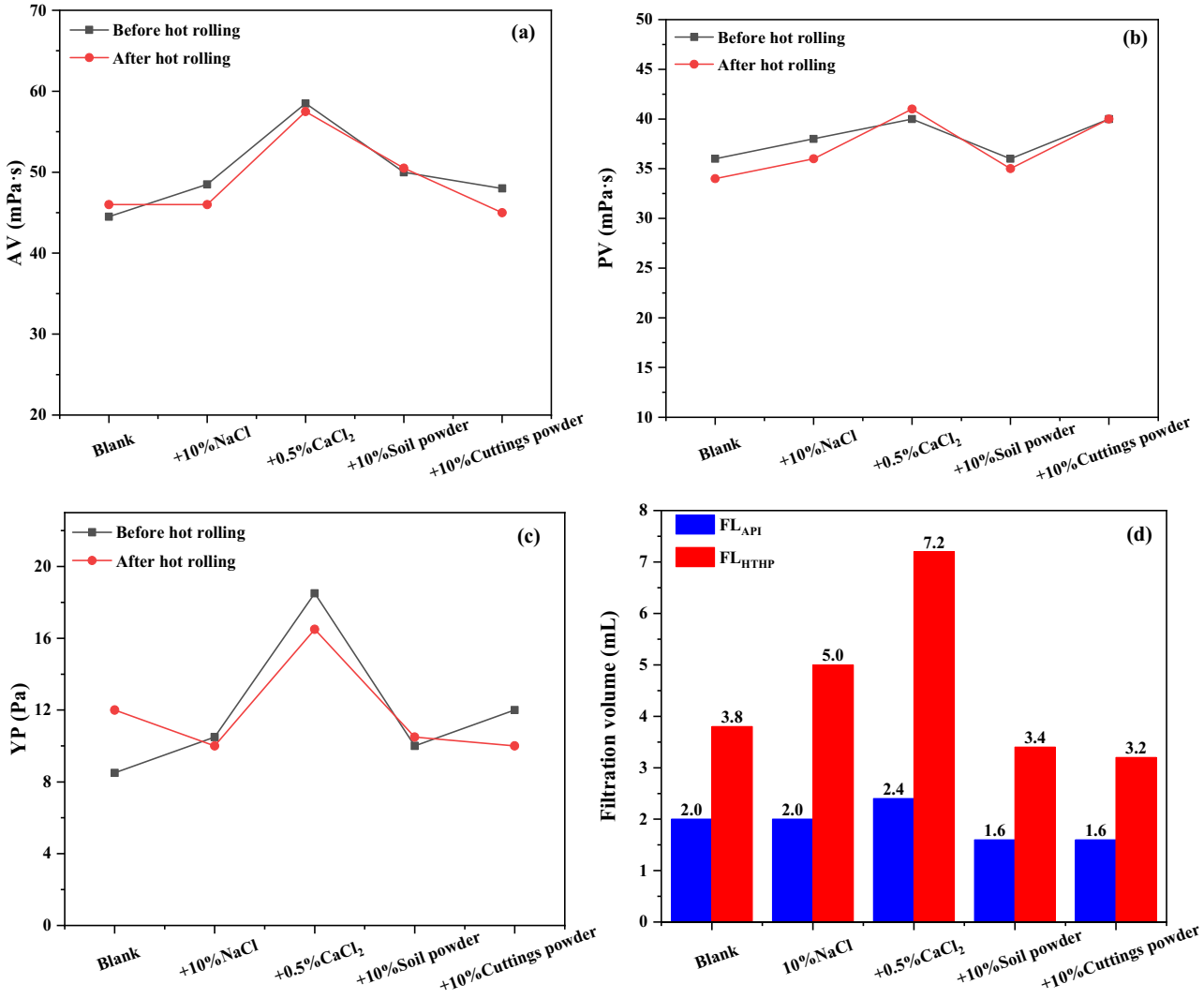

Figure 12: The rheological properties and fluid-loss control performance of SA-WBDF and SA-WBDFs contaminated with different pollutants. AV (a); PV (b); YP (c); and FL_{API} and FL_{HTHP} (d).

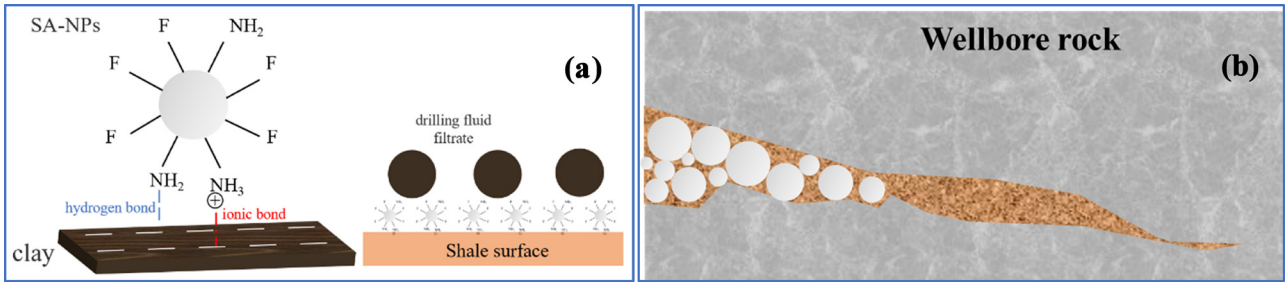

Figure 13: The mechanism of using SA-NPs to improve shale stability. Adsorption and wetting characteristics of SA-NPs on the shale surface (a) and plugging function of SA-NPs (b).

drilling process, and can properly face various complex formations, such as salt-gypsum formation.

3.6 Mechanism analysis

Generally, shale is rich in clay minerals and exhibits strong amphiphilicity. Meanwhile, given lots of nano-micro pores and cracks on its surface, its strong capillary self-priming effect [41] allows the drilling fluid filtrate to easily penetrate the shale through pores and cracks under the bottom hole pressure difference and capillary force. Free water in the filtrate causes the hydration swelling of the clay minerals. At the same time, the oil-soluble components such as lubricants, hydrophobic polymers, and mineral oil in the filtrate weaken the cohesion between clay mineral particles. Furthermore, the intrusion of filtrate increases the pore pressure of wellbore rock, resulting in the expansion and widening of the original fractures. These factors may bring a decrease in wellbore rock strength and the destruction of the stress balance, resulting in wellbore instability [42]. Modified by amine groups, the surface of SA-NPs could be attached strongly to the shale surface through ionic bonding and hydrogen bonding [43]. Due to its nanoscale "coalesce" structure, the shale surface adsorbed with SA-NPs would exhibit a nano-papillary structure, significantly improving its surface roughness at the nano-micro scale. Coupled with the presence of ultra-low surface energy components (halothane segments), the SA-NPs-treated shale exhibited super-amphiphobic surface property, thus avoiding the binding of water molecules to clay minerals and preventing the penetration of drilling fluid filtrate into the shale (Figure 13a). Also, since SA-NPs have sizes between 70 and 200 nm, they can plug the nano-micron pores and cracks on the shale surface through bridging and accumulation to further avoid the invasion of filtrate (Figure 13b). The addition of SA-NPs could further avoid the hydration swelling of wellbore rock, inhibit the hydration dispersion of shale cuttings, and

Table 4: Drilling parameters of Well (A) and Well (B)

Well name	ECD	Expansion rate of wellbore diameter/%	Drilling cycle/day	Accidents during drilling
Well (A)	1.58–1.62	5.62	11.5	—
Well (B)	1.78–1.72	7.35	20.97	Peeling and block dropping, sticking, etc

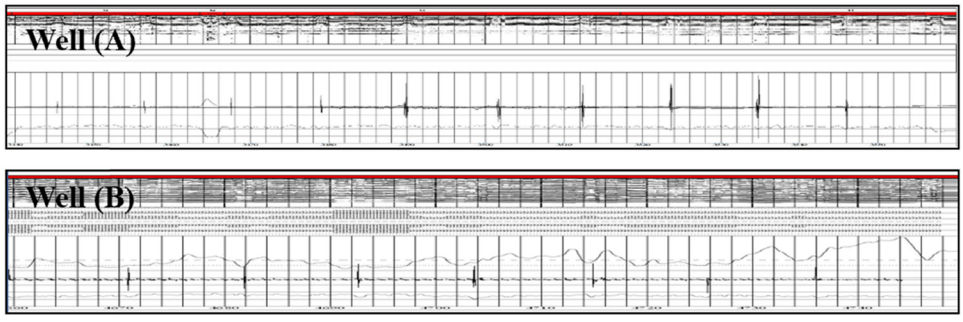

Figure 14: Well logging data of Well (A) and Well (B).

prevent the transmission of filtrate pressure, improving the wellbore rock strength and stability.

4 Field application

Well (A), located in the fault nose structure of Liujianfang area in Dagang Oilfield, is a horizontal well for target reservoir Ban 4. Given safety concerns in drilling through troublesome Sha 1 shale formations, the operation used KCl/PHPA drilling fluid first. Nevertheless, when the drilling operation reached the upper shale formation of Sha 1, serious peeling and block dropping occurred, leading to complex situations such as borehole diameter expanding, sticking, and wellbore collapse. To prevent further deterioration of the wellbore instability, many efforts such as increasing the amount of amino-based inhibitor, asphalt powder, and raising mud density were made, but the results remained grim.

Based on the excellent shale stabilization performance, SA-WBDFs were selected as the drilling fluid for continuous drilling in this section. As shown by the results of the real-time drilling monitor, the peeling and block dropping issues were apparently reduced after changing KCl/PHPA drilling fluid with SA-WBDFs. Finally, the Sha 1 formation was drilled successfully, during which no wellbore instability, sticking, and other complex situations occurred. The drilling parameters and well logging data of Well (A) using SA-WBDFs and Well (B) using PHPA/KCl drilling fluid in the same work area are shown in Table 4 and Figure 14. As shown in Table 4, compared to adjacent Well (B) that used PHPA/KCl as drilling fluid, Well (A) had a smaller drilling cycle but equivalent circulating density (ECD) and expansion rate of wellbore diameter and encountered no downhole problems. In further comparison, as shown in the logging data in Figure 14, Well (A) has a smaller diameter change and a more regular borehole. The difference was caused by the use of SA-WBDFs that reversed the wettability of the rock surface of Sha 1 formation, avoided the capillary self-priming effect, and effectively plugged the pores and cracks on the wellbore rock surface, thereby significantly minimizing the negative impact of WBDFs on the wellbore rock strength.

5 Summary and conclusions

(1) Aiming at the wellbore instability issue in drilling shale wells, SA-NPs were investigated systematically and used to enhance the wellbore stabilization performance of WBDFs.
(2) SA-NPs could be adsorbed on the surface of shale to form a nano-micro scale rough structure, which alters the wettability of the shale surface and the direction of capillary force and prevents the water/oil phase from intruding into the shale.
(3) By adding 1 wt% SA-NPs, the WBDFs showed great improvement in linear swelling test, hot-rolling recovery experiment, plugging rate test, and HTHP uniaxial compressive strength test.
(4) The application in Dagang Oilfield further proved that WBDFs with SA-NPs could address wellbore instability in shale formation and have a good application prospect.

Nomenclature

API	American Petroleum Institute
AV	apparent viscosity
$CaCl_2$	calcium chloride
ECD	equivalent circulating density
Eq	equation
FL	filtration volume
h_t	final height of shale cuttings pellet after immersed in test liquids for a certain time
h_0	initial height of shale cuttings pellet
HTHP	high-temperature and high-pressure
IEDFs	invert emulsion drilling fluids
KCl/PHPA	potassium chloride/partially hydrolyzed polyacrylamide
K_i	permeability of the original shale core
K_p	permeability of the shale core contaminated with drilling fluids
m_1	remaining mass of the shale cuttings
m_0	original mass of the shale cuttings
NaCl	sodium chloride
p_c	capillary force
PDMDAAC	poly dimethyldiallyl ammonium chloride
P_r	plugging rate
PV	plastic viscosity
r	capillary radius
SA-NPs	super-amphiphobic nano-silica nanoparticles
SEM	scanning electron microscopy
SiO_2	fumed silica nanoparticles
TEM	transmission electron microscopy
WBDFs	water-based drilling fluids
w/v	weight/volume

YP	yield point
ρ	density
σ	surface tension of deionized water
θ	contact angle of capillary inner surface
θ_{600}	Dial readings of the viscometer at 600 rpm
θ_{300}	Dial readings of the viscometer at 300 rpm

Acknowledgements: The authors would like to acknowledge financial support from the National Natural Science Foundation of China.

Funding information: This work was supported by the National Natural Science Foundation (Grant No. 51874329 and Grant No. 51991361) and the National Natural Science Innovation Population of China (Grant No. 51821092).

Author contributions: Xuwu Luo: conceptualization, methodology, investigation, data curation, formal analysis, and writing – original draft; Guancheng Jiang: methodology, project administration, supervision, resources, and writing – original draft; Guoshuai Wang: methodology, resources, and writing – review and editing; Lili Yang: supervision, conceptualization, and writing – review and editing; Yinbo He: methodology; Kaixiao Cui: writing – review and editing; Jun Yang: writing – review and editing.

Conflict of interest: There are no conflicts to declare.

Data availability statement: The data used to support the findings of this study have not been made available because they also form part of an ongoing study.

References

[1] Li, M., Q. Wu, J. Han, C. Mei, T. Lei, S. Lee, et al. Overcoming salt contamination of bentonite water-based drilling fluids with blended dual-functionalized cellulose nanocrystals. *ACS Sustainable Chemistry & Engineering*, Vol. 31, No. 8, 2020, pp. 11569–11578.

[2] Ross, D. J. K. and R. M. Bustin. The importance of shale composition and pore structure upon gas storage potential of shale gas reservoirs. *Marine & Petroleum Geology*, Vol. 26, No. 6, 2009, pp. 916–927.

[3] Curtis, J. B. Fractured shale-gas systems. *AAPG Bulletin*, Vol. 86, No. 11, 2002, pp. 1921–1938.

[4] Labani, M. M., R. Rezaee, A. Saeedi, and A. A. Hinai. Evaluation of pore size spectrum of gas shale reservoirs using low pressure nitrogen adsorption, gas expansion and mercury porosimetry: a case study from the perth and canning basins, western australia. *Journal of Petroleum Science & Engineering*, Vol. 112, 2013, pp. 7–16.

[5] Fan, X., M. Zhang, Q. Zhang, P. Zhao, B. Yao, and D. Lv. Wellbore stability and failure regions analysis of shale formation accounting for weak bedding planes in ordos basin. *Journal of Natural Gas Science and Engineering*, Vol. 77, 2020, id. 103258.

[6] Li, X., G. Jiang, J. Wang, and X. Ni. Inhibitive properties comparison of different polyamino acids in water-based drilling fluids. *Journal of Natural Gas Science and Engineering*, Vol. 83, 2020, id. 103589.

[7] Huang, W., H. Zhong, J. Cao, and Z. Qiu. Poly (oxypropylene)-amidoamine modified bentonite as potential shale inhibitor in water-based drilling fluids. *Applied Clay Science*, Vol. 67–68, 2012, pp. 36–43.

[8] Anderson, R. L., I. Ratcliffe, H. C. Greenwell, P. A. Williams, S. Cliffe, and P. V. Coveney. Clay swelling – a challenge in the oilfield. *Earth Science Reviews*, Vol. 98, No. 3, 2010, pp. 201–216.

[9] Leite, R. S., A. P. T. Dantas, and L. V. Amorim. Influence of clay swelling inhibitor in filtration properties of water-based drilling fluids. *Materials Science Forum*, Vol. 869, 2016, pp. 1018–1022.

[10] Kelly, J. Drilling fluids selection, performance, and quality control. *Journal of Petroleum Technology*, Vol. 35, No. 5, 1983, pp. 889–898.

[11] Zhou, L., J. Feng, J. Lei, and J. Yuan. Experimental application of salt slurry in zhongyuan high density polymer saturated brine-based drilling fluid. *Advanced Materials Research*, Vol. 335–336, 2011, pp. 1348–1351.

[12] Guo, J., J. Yan, W. Fan, and H. Zhang. Applications of strongly inhibitive silicate-based drilling fluids in troublesome shale formations in sudan. *Journal of Petroleum Science and Engineering*, Vol. 50, No. 3, 2006, pp. 195–203.

[13] Xiong, Z., S. Tao, X. Li, W. Shan, and H. Dong. Development and application of anti-collapse & anti-drag agent for drilling fluid. *Procedia Engineering*, Vol. 73, 2014, pp. 55–62.

[14] Cao, J., T. Song, Y. Zhu, S. Wang, X. Wang, F. Lv, et al. Application of amino-functionalized nanosilica in improving the thermal stability of acrylamide-based polymer for enhanced oil recovery. *Energy & Fuels*, Vol. 32, No. 1, 2017, pp. 246–254.

[15] He, Y., G. Jiang, and W. Cui. Salt-responsive AM/AMPS/ATC terpolymers as modifiers for rheology and fluid loss in water-based drilling fluid. *Key Engineering Materials*, Vol. 765, 2018, pp. 106–112.

[16] He, Y., G. Jiang, Z. Deng, F. Liu, S. Peng, X. Ni, et al. Polyhydroxy gemini surfactant as a mechanoresponsive rheology modifier for inverted emulsion drilling fluid. *RSC Advances*, Vol. 8, 2018, pp. 342–353.

[17] Huang, X., G. Jiang, Y. He, Y. An, and S. Zhang. Improvement of rheological properties of invert drilling fluids by enhancing interactions of water droplets using hydrogen bonding linker. *Colloids and Surfaces A Physicochemical and Engineering Aspects*, Vol. 506, 2016, pp. 467–475.

[18] Mao, H., Y. Yang, H. Zhang, J. Zheng, and Y. Zhong. Conceptual design and methodology for rheological control of water-based drilling fluids in ultra-high temperature and ultra-high pressure drilling applications. *Journal of Petroleum Science and Engineering*, Vol. 188, 2020, id. 106884.

[19] Wang, K., G. Jiang, X. Li, and P. F. Luckham. Study of graphene oxide to stabilize shale in water-based drilling fluids. *Colloids*

and Surfaces A Physicochemical and Engineering Aspects, Vol. 606, 2020, id. 125457.
[20] Jiang, G., K. Wang, Y. He, L. Yang, and Y. Deng. Synthesis of an amphoteric polymer as a high-temperature-resistant shale stabilizer in water-based drilling fluids. *Journal of Applied Polymer Science*, Vol. 137, No. 35, 2020, id. 49016.
[21] Wong, W. S. Y. Surface chemistry enhancements for the tunable super-liquid repellency of low-surface-tension liquids. *ACS AuthorChoice*, Vol. 19, No. 3, 2019, pp. 1892–1901.
[22] Safari, M., R. Gholami, C. X. Liew, A. Raza, and J. V. Vettaparambil. A new mud design to reduce formation damage in sandstone reservoirs. *Journal of Petroleum Science and Engineering*, Vol. 181, 2019, id. 106221.
[23] Shi, Y., S. Chen, Y. Peng, J. Song, and J. Cai. Experimental study on synergistically enhancing the wellbore stability of coal measure strata by electrical inhibition and neutral wetting. *Meitan Xuebao/Journal of the China Coal Society*, Vol. 43, No. 6, 2018, pp. 1701–1708.
[24] Shi, Y., S. Chen, X. Yang, L. Yu, and J. Cai. Enhancing wellbore stability of coal measure strata by electrical inhibition and wettability control. *Journal of Petroleum Science and Engineering*, Vol. 174, 2019, pp. 544–552.
[25] Xu, J., Z. Qiu, X. Zhao, and W. Huang. Hydrophobic modified polymer-based silica nanocomposite for improving shale stability in water-based drilling fluids. *Journal of Petroleum Science and Engineering*, Vol. 153, 2017, pp. 325–330.
[26] Yue, Y., S. Chen, Z. Wang, X. Yang, Y. Peng, J. Cai, et al. Improving wellbore stability of shale by adjusting its wettability. *Journal of Petroleum Science and Engineering*, Vol. 161, 2018, pp. 692–702.
[27] Cheraghian, G., M. Hemmati, and S. Bazgir. Application of TiO_2 and fumed silica nanoparticles and improve the performance of drilling fluids. *AIP Conference Proceedings*, *American Institute of Physics*, 2014, pp. 266–270.
[28] Cheraghian, G. Nanoparticles in drilling fluid: A review of the state-of-the-art. *Journal of Materials Research and Technology*, Vol. 13, No. 11, 2021, pp. 737–753.
[29] Ikram, R., B. M. Jan, A. Sidek, and G. Kenanakis. Utilization of eco-friendly waste generated nanomaterials in water-based drilling fluids; state of the art review. *Materials*, Vol. 14, No. 15, 2021, id. 4171.
[30] Ahmed, W., M. Booth, and E. Nourafkan. Emerging nanotechnologies for renewable energy. *Chapter 6 - Nanotechnology for drilling operations*, ed. G. Cheraghian, Afrand, M., Elsevier Inc, Amsterdam, 2021, 135-148
[31] Schmüser, L., N. Encinas, M. Paven, D. J. Graham, D. G. Castner, D. Vollmer, et al. Candle soot-based superamphiphobic coatings resist protein adsorption. *Biointerphases*, Vol. 11, No. 3, 2016, id. 031007.
[32] Huang, Y., Z. Wang, D. Hou, and S. Lin. Coaxially electrospun super-amphiphobic silica-based membrane for anti-surfactant-wetting membrane distillation. *Journal of Membrane Science*, Vol. 531, 2017, pp. 122–128.
[33] Wei, J., B. Li, L. Jing, N. Tian, X. Zhao, and J. Zhang. Efficient protection of mg alloy enabled by combination of a conventional anti-corrosion coating and a superamphiphobic coating. *Chemical Engineering Journal*, Vol. 390, 2020, id. 124562.
[34] Yuan, R., S. Wu, H. Wang, L. Hu, Y. Zhu, S. Gao, et al. Facile fabrication approach for a novel multifunctional superamphiphobic coating based on chemically grafted montmorillonite/Al_2O_3-polydimethylsiloxane binary nanocomposite. *Journal of Polymer Research*, Vol. 24, No. 4, 2017, id. 10965.
[35] Hu, M., H. J. Butt, K. Landfester, M. B. Bannwarth, S. Wooh, and H. Thérien-Aubin. Shaping the assembly of superparamagnetic nanoparticles. *ACS AuthorChoice*, Vol. 13, No. 3, 2019, pp. 3015–3022.
[36] Wan, Y., L. Xu, Z. Liu, and H. Yu. Fabrication of a superamphiphobic aluminium alloy surface via wire electrical discharge machining and chemical etching technology. *IET Micro & Nano Letters*, Vol. 12, No. 3, 2017, pp. 175–178.
[37] Sheen, Y. C., Y. Huang, C. Liao, H. Chou, and F. Chang. New approach to fabricate an extremely super-amphiphobic surface based on fluorinated silica nanoparticles. *Journal of Polymer Science Part B Polymer Physics*, Vol. 46, No. 18, 2010, pp. 1984–1990.
[38] Wang, H., H. Zhou, H. Niu, J. Zhang, Y. Du, and T. Lin. Dual-layer superamphiphobic/superhydrophobic-oleophilic nanofibrous membranes with unidirectional oil-transport ability and strengthened oil-water separation performance. *Advanced Materials Interfaces*, Vol. 2, No. 4, 2015, id. 1400506.
[39] Zhang, Y., H. Xia, E. Kim, and H. Sun. Recent developments in superhydrophobic surfaces with unique structural and functional properties. *Soft Matter*, Vol. 8, No. 44, 2018, pp. 11217–11231.
[40] Lu, Y., S. Sathasivam, J. Song, C. R. Crick, and I. P. Parkin. Robust self-cleaning surfaces that function when exposed to either air or oil. *Science*, Vol. 347, No. 6225, 2015, pp. 1132–1135.
[41] Ni, X., G. Jiang, F. Liu, and Z. Deng. Synthesis of an amphiphobic nanofluid with a novel structure and its wettability alteration on low-permeability sandstone reservoirs. *Energy & Fuels*, Vol. 32, No. 4, 2018, pp. 4747–4753.
[42] Ni, X., G. Jiang, Y. Li, L. Yang, W. Li, K. Wang, et al. Synthesis of superhydrophobic nanofluids as shale inhibitor and study of the inhibition mechanism. *Applied Surface Science*, Vol. 484, 2019, pp. 957–965.
[43] Jiang, G. *Gas wettability of reservoir rock surfaces with porous media*, Gulf Professional Publishing, Cambridge, MA, 2018.
[44] Guo, X., Y. Zhang, and X. Cheng. In-situ fluorinating silica nanoparticles for superamphiphobic coating preparation. *Journal of The Chinese Ceramic Society*, Vol. 48, No. 1, 2020, pp. 128–134.
[45] Feng, X. and L. Jiang. Design and creation of superwetting/antiwetting surfaces. *Advanced Materials Technologies*, Vol. 18, No. 23, 2006, pp. 3063–3078.
[46] Yang, L., G. Jiang, Y. Shi, X. Lin, and X. Yang. Application of ionic liquid to a high-performance calcium-resistant additive for filtration control of bentonite/water-based drilling fluids. *Journal of Material Science*, Vol. 52, 2017, pp. 6362–6375.